Available online at www.sciencedirect.com
SCIENCE DIRECT®
Journal of Theoretical Biology 229 (2004) 455–476
Journal of Theoretical Biology
www.elsevier.com/locate/jtbi

A general mathematical framework to model generation structure in a population of asynchronously dividing cells

Kalet León[a,b,*], Jose Faro[b], Jorge Carneiro[b]

[a] Centro de Inmunología Molecular, Habana, Cuba
[b] Instituto Gulbenkian de Ciência, Rua da Quinta Grande, No 6, Apartado 14, P-2781-901, Oeiras Cedex, Portugal

Received 30 July 2003; received in revised form 28 February 2004; accepted 8 April 2004

Abstract

In otherwise homogeneous cell populations, individual cells undergo asynchronous cell cycles. In recent years, interest in this fundamental observation has been boosted by the wide usage of CFSE, a fluorescent dye that allows the precise estimation by flow cytometry of the number of divisions performed by different cells in a population, and thus the generation structure. In this work, we propose two general mathematical frameworks to model the time evolution of generation structure in a cell population. The first modeling framework is more descriptive and assumes that cell division time is distributed in the cell population, due to intrinsic noise in the molecular machinery in individual cells; while the second framework assumes that asynchrony in cell division stems from randomness in the interactions individual cells make with environmental agents. We reduce these formalisms to recover two preexistent models, which build on each of the hypotheses. When confronted to kinetics data on CFSE labeled cells taken from literature, these models can fit precursor frequency distributions at each measured time point. However, they fail to fit the whole kinetics of precursor frequency distributions. In contrast, two extensions of those models, derived also from our general formalisms, fit equally well both the whole kinetics and individual profiles at each time point, providing a biologically reasonable estimation of parameters. We prove that the distribution of cell division times is not Gaussian, as previously proposed, but is better described by an asymmetric distribution such as the Gamma distribution. We show also that the observed cell asynchrony could be explained by the existence of a single transitional event during cell division. Based on these results, we suggest new ways of combining theoretical and experimental work to assess how much of noise in internal machinery of the cell and interactions with the environmental agents contribute to the asynchrony in cell division.

Keywords: Cell cycle analysis; Modeling cell proliferation; CFSE technique

1. Introduction

Individual cells in a population divide with different division times, leading to a wide distribution in terms of generation numbers at distinct times after stimulation. In spite of being the focus of much research, the basis for such asynchrony of cell division constitutes a long enduring problem that remains yet to be solved. Two alternative hypotheses were considered in the past to explain asynchronous division. On the one hand, Koch and Schaechte, 1962) proposed that asynchrony would stem from the intrinsic heterogeneity in the initial population of cells. On the other hand, Burns and others (Burns & Tannock, 1970; Smith & Martin, 1974) hypothesized that the initial cell population is homogeneous and asynchrony arises from the stochastic nature of extra-cellular interactions affecting cell division. Considerable effort was devoted in the past to distinguish among these hypotheses (Arino, 1995; Burns & Tannock, 1970; Darzynkiewicz et al., 1982; Koch, 1980; Kubitschek, 1970; Smith & Martin, 1974), with no conclusive results. A milestone in this field was the discovery of IL-2 physiology in lymphocyte proliferation by Cantrell and Smith, 1984),

*Corresponding author. Instituto Gulbenkian de Ciencia, Rua da Quinta Grande, No. 6, Apartado 14, P-2781-901 Oeiras Codex, Portugal. Tel.: 351-214-407-920; fax: 351-214-407-973/970.
E-mail addresses: kalet@ict.cim.sld.cu, kleon@icg.gulbenkian.pt (K. León).

0022-5193/$ - see front matter © 2004 Elsevier Ltd. All rights reserved.
doi:10.1016/j.jtbi.2004.04.011

which allowed the practical synchronization of cell division. Based on this finding they suggested that asynchrony was due to the naturally distributed surface expression of the IL-2 receptor on stimulated lymphocytes. However, these studies have always suffered from a lack of a quantitative assay that allowed the precise estimation of the number of cell divisions performed by the different cells in a population and their distribution at different times.

A recent technique based on the 5- (and 6-) carboxyfluorescein diacetate succinimidyl ester (CFSE) fluorescent dye affords a precise way to directly quantitate asynchrony in cell division. CFSE attaches covalently to the aminas in the cytoplasm of the labeled cells and is distributed evenly among its daughter cells upon mitosis, i.e. in each generation the concentration of CFSE is halved (Lyons and Parish, 1994). This dye allows thus the quantitative distinction, by flow cytometry, of cells according to the number of citokinesis they have undergone (generation number) given that the progenitor cells were homogeneously labeled. This fluorescence method can be complemented to simultaneously address issues on cell differentiation (Hasbold et al., 1999). Results using this technique typically show a broad multimodal distribution of cells according to fluorescence intensity and consequently according to their generation.

This technique could represent a promise to resolve the issue of quantifying the relative contributions of intrinsic noise in the cellular machinery or randomness in extra-cellular interactions for the asynchrony in cell division. However, these quantitative studies will require appropriate mathematical modeling. A few mathematical models have been recently advanced attempting at a quantitative analysis of the results of CFSE experiments. On the one hand, Gett and Hodgkin, 2000) and Hasbold et al. (1999) fitted Gaussian distributions to the CFSE-generation structure. The interpretation for the asynchrony of cell division in this model was the existence of an intrinsic cellular noise in the processes controlling the first round of division, clearly relating to the theoretical hypothesis of Koch and Schaechte, 1962). On the other hand, Nordon et al. (1999), proposed a simple cell cycle model that explicitly includes the process of cell activation upon interaction with extra-cellular ligands, being the stochastic nature of the activating interactions the cause for asynchronous cell division, as proposed by Burns and others (Burns and Tannock, 1970; Smith and Martin, 1974). These models have been claimed to satisfactorily explain specific CFSE experimental data, however, as we show here, they lack in generality. Hence, for the data used here, the previously proposed models fit independently the generation distribution of proliferating T cells for any measured time point, but fail to fit simultaneously the whole kinetics of those distributions.

In this context, the goal of the present article is to provide general mathematical models to properly analyse data on the time evolution of CFSE-based generation structures. To this end, we first formulate two general mathematical frameworks. The first framework is more descriptive and assumes that cell division times are distributed in a cell population as expected if the intracellular, molecular machinery controlling cell cycle in individual cells had a stochastic component (Section 3.1). The second framework is more mechanistic and assumes that heterogeneity in cell division times stems from randomness in the interactions the cell makes with its environment and that control cell cycle progression (Section 4.1). From these general frameworks we derive as specific cases the Gett–Hasbold (Section 3.2) and Nordon (Section 4.2) models, showing than they fail to explain the evolution in time of the CFSE profiles. Then, we propose more accurate and generic models (Sections 3.3 and 4.3) discussing their biological significance. Finally (Section 5) we discuss how the present analysis cannot allow us to assess the cause(s) of asynchrony of cell division, but it provides some clues on how to progress in that direction.

2. Material and methods

2.1. The precursor frequency distribution in CFSE profiles

The basic result of a CFSE assay is a profile or histogram of the frequency of cells as a function of their CFSE fluorescence intensity. In an ideal profile, those cells that belong to the mth generation (i.e. the cells that have undergone m division rounds since their original labeling) can be resolved from those of the generations $m-1$ and $m+1$. Under those conditions one can obtain the frequency of cells in each generation m, denoted $f(m,t)$, in a sample of a cell population that was growing for a period t since labeling and stimulation.

Assuming that cell death does not differ from generation to generation, a precursor frequency in each generation at time t ($W(m,t)$) can be estimated from the frequency of cells in each generation (Givan et al., 1999) as

$$W(m,t) = \frac{f(m,t)}{2^m} \Bigg/ \sum_{k=0}^{\infty} \frac{f(k,t)}{2^k}. \tag{1}$$

This quantity is a discrete distribution that can be calculated directly from the peak areas in the experimental CFSE profiles, and we will refer to it as the precursor frequency distribution for a given CFSE profile.

Although we will refer to the quantity computed according to Eq. (1) as "precursor frequency" it is worth noticing that this is an effective precursor frequency, which underestimates the true precursor frequency for the cells in each generation. The following example can clarify this statement. Consider 10 cells labeled with CFSE. Let us assume that one and only one of these cells has undergone a round of division and that one of its daughter cells has undergone also one round of division. Under these conditions we have 9 undivided cells, 1 cell in the first generation and 2 in the second generation. Clearly, in this simple example the precursor frequency is 0.1. How many cells are precursors of the cell in the first generation? and in the second generation? The obvious answer to both these questions is 'one cell', and therefore the precursor frequency of the cells in the first generation is 0.1 and the precursor frequency of second generation cells is also 0.1. In contrast, the quantity computed with Eq. (1) will be 0.05 for both first and second generations. However, the sum of the effective "precursor frequencies" over all generations gives the true precursor frequency of the population.

2.2. Experimental data

The models were tested against two data sets obtained from the literature (Gett & Hodgkin, 2000). Briefly, these data sets were obtained as follows: naive CD4+ T cells (small $CD62L^{hi}CD44^{lo}CD25$-) were labeled with CFSE and stimulated with immobilized monoclonal antibody (mAb) to CD3 (anti-CD3, 10 μg/ml) and IL-2 (100 U/ml) in the absence (data set #1) or presence (data set #2) of anti-CD28 mAb. After various culture times (36, 48, 60, 72, 84, 96, 108 hours) the CFSE profiles were scored and the distribution of precursor frequencies corresponding to these profiles was determined (see Table 1). Those data sets provide therefore the kinetics of the precursor frequency distributions in the absence or presence of co-stimulatory signals through CD28.

2.3. Fitting of the models to experimental data

Several models are proposed and evaluated here by their capacity to fit the whole kinetic process in a given data set and not each individual time point distribution as previously done (Gett and Hodgkin, 2000; Hasbold et al., 1999). Given the large number of parameters in the models, the fittings are performed in a two-step procedure. First, the time evolution of the frequency of undivided cells is fitted, by minimizing the following function:

$$\chi_0^2 = \sum_{n=0}^{N_t} \frac{(W(0,t_n) - w(0,t_n))^2}{\varepsilon(0,t_n)}, \tag{2}$$

where the introduced quantities are defined in Table 2.

This first step provides good estimates of parameters controlling the dynamics of the first round of division in each particular model. These estimates are then used as a starting point in the second step, where the data set is fitted as a

Table 1
Experimental precursor frequency distributions

t (h)	$n=0$	$n=1$	$n=2$	$n=3$	$n=4$	$n=5$	$n=6$	$n=7$	$n=8$
Precursor frequency distribution ($W(n,t)$)*: data set #1*									
36	0.94	0.06	0.0	—	—	—	—	—	—
48	0.77	0.22	0.01	0.0	—	—	—	—	—
60	0.61	0.28	0.10	0.0	—	—	—	—	—
72	0.43	0.27	0.21	0.07	0.01	0.0	—	—	—
84	0.39	0.23	0.22	0.12	0.04	0.0	—	—	—
96	0.28	0.15	0.20	0.20	0.12	0.04	0.01	0.0	—
108	0.24	0.12	0.14	0.20	0.19	0.08	0.02	0.0	—
Precursor frequency distribution ($W(n,t)$)*: data set #2*									
t (h)	$n=0$	$n=1$	$n=2$	$n=3$	$n=4$	$n=5$	$n=6$	$n=7$	$n=8$
36	0.93	0.07	0.0	—	—	—	—	—	—
48	0.52	0.38	0.09	0.0	—	—	—	—	—
60	0.42	0.31	0.21	0.06	0.0	—	—	—	—
72	0.18	0.21	0.34	0.20	0.07	0.0	—	—	—
84	0.15	0.09	0.20	0.26	0.20	0.08	0.02	0.0	—
96	0.12	0.05	0.12	0.21	0.26	0.16	0.06	0.01	0.0
108	0.14	0.05	0.06	0.15	0.23	0.20	0.12	0.04	0.01

Table 2
Quantities in Section 2.2

Quantity	Quantity definition
$W(m,t)$	Experimentally determined distribution of precursor frequencies at the given time point (t)
$W(m,t)$	Theoretically predicted distribution of precursor frequencies at the given time point t
$N_p(t)$	Maximal number of division rounds observed at time t
N_t	Number of time points in the kinetic series
t_i	Time point i in the kinetic experiment
$\varepsilon(m,t)$	Function weighting the contribution to the overall fitting of each generation in the distribution.

whole by minimizing the following function:

$$\chi^2 = \sum_{n=0}^{N_t} \sum_{m=0}^{N_p(t_n)} \frac{(W(m,t_n) - w(m,t_n))^2}{\varepsilon(m,t_n)}. \tag{3}$$

Again, the introduced quantities are defined in Table 2.

Note that all model parameters are adjusted in this second fitting step. We take advantage of the fact that the first step provides initial values for a subset of the parameters that are close to the real solution. Using those initial values speeds up the convergence of algorithm, and in so doing allows exploring a larger range of initial values of the remaining parameters. Moreover, this procedure turns out to be informative in the analysis of the models as will be shown in Section 4.

The best-fit parameters in each model are obtained in this second step, and depend on the particular choice of the function $\varepsilon(m,t)$. This function weights the contribution of each individual frequency in the data to the overall fitting. In principle, this quantity should be taken proportional to the error in determining the area of the corresponding experimental peak in the profile. However, in the absence of an experimental estimation of these errors, we assume $\varepsilon(m,t)$ as the following function of the precursor frequency:

$$\varepsilon(m,t) = \varepsilon_a + \varepsilon_r W(m,t), \tag{4}$$

where ε_a and ε_r are interpreted, respectively, as the minimal absolute and relative error in any given experimental determination of an individual frequency. In this paper, ε_a and ε_r were set to the values 0.01 and 0.05, respectively. Changes in the values of ε_a and ε_r lead to only small changes of the best-fit parameters of the different models (data not shown), such that the main conclusions on model comparison remain valid.

The numerical computations of the fitting procedure were performed with the software Mathematica 3.0 (Wolfram Inc). The FindMinimum function of this software was used with 1000 initial parameter sets randomly generated inside a reasonable interval of values. Such procedure was set to avoid local minima. In our hands, it leads typically to 3–5 different local minima, where the reported best-fit here was systematically reached in more than 25% of the trials.

2.4. Statistical significance of the fittings

The statistical significance of the fittings was assessed by assuming that individual frequencies in the precursor frequency distribution were independent and with determination errors that comply a normal distribution. Under these assumptions, the significance of the fitting can be easily evaluated since the $\chi^2(t)$ function (Eq. (3)) follows the classical χ^2 distribution of dimension $\sum_{n=1}^{N_t} N_p(t_n)$ minus the number of independent parameters in the model. However, the fitting significance obviously depends on the parameters ε_a and ε_r through the error weighting function $\varepsilon(m,t)$. Therefore, instead of looking for the absolute significance of a fitting, the models are compared in respect to the minimal relative error (values of ε_r) needed to make the fitting significant with 95% confidence.

A confidence interval was also computed for each estimated parameter, using a simple bootstrapping algorithm as described by Press et al. (1999). Briefly several re-sampling of the distribution of frequency errors were done. For each re-sampled distribution a set of best-fit parameters was obtained, being sorted according to the fitting quality. The confidence interval for each parameter was estimated as its maximum variation range among the best 95% of these fittings.

3. Modeling the generation-structure of a cell population with distributed division times

3.1. A general framework

Let us consider a population of cells where heterogeneity of division times upon stimulation is due to the intrinsic noise of the intracellular machinery controling cell cycle. In this case heterogeneous cell division can be described defining a set of probability distributions $P_n(t_r)$ for the probability that a cell in generation $n-1$ undergoes nth division round in the time t_r. That is, P_n is the probability distribution of residence times (t_r) of cells in generation $n-1$. Given such set of distributions for a population of cells, the probability distribution $L_n(t)$ for the probability that a cell divides n times in the time t can be obtained recursively as

$$\begin{aligned} L_1(t) &= P_1(t), \\ L_2(t) &= \int_0^t P_2(t-x)L_1(x)\,\mathrm{d}x, \\ &\vdots \\ L_n(t) &= \int_0^t P_n(t-x)L_{n-1}(x)\,\mathrm{d}x \end{aligned} \tag{5}$$

and the probability of having divided at least n times at time t *after stimulation* is obtained as

$$H_n(t) = \begin{cases} 1 & \text{if } n = 0, \\ \int_0^t L_n(x)\,\mathrm{d}x & \text{if } n > 0. \end{cases} \tag{6}$$

Using the latter quantity and assuming that cells in different generations die exponentially in the culture with a rate constant k_d (i.e. cell death is independent of division history) the expected number of cells recovered in generation n at time t after stimulation (denoted $N_n(t)$) is obtained as

$$N_n(t) = 2^n N_0(H_n(t) - H_{n+1}(t))E^{-k_d t}, \tag{7}$$

where N_0 is the total number of cells at the beginning of the culture.

Finally following its definition (Section 2.1), the expected precursor frequencies in a single cell population (denoted $w_n(t)$) is given by

$$w_n(t) = (H_n(t) - H_{n+1}(t)). \tag{8}$$

Lets now consider a more general case where the initial culture contains k different subpopulations of cells (label i from 0 to k). Each subpopulation represents initially a fraction f_l of the total cell numbers and the division times of its cells follow a specific probability distribution $P_n^l(t)$. In this case, assuming that different subpopulations divide independently in the culture, the precursor frequency of cells in generation n at time t after stimulation is easily obtained as follows:

$$w_n(t) = \sum_{i=1}^{k} f_i w_n^i(t), \tag{9}$$

where $w_n^i(t)$ is calculated according to Eq. (8) using the specific probability distribution of division time of each subpopulation i $P_n^i(t)$.

Eq. (9) provides a general mathematical framework to model the results of CFSE assays, where the number of different populations and the shape of the probability distributions $P_n^i(t)$ have to be specified, before practical application. Two particular realizations of this formalism are derived in the following sections and used to analyse experimental data of Section 2.2.

3.2. Gett–Hasbold model: cell division times are normal distributed

To recover the Gett–Hasbold model (G–H) from the above general formalism it is first required to make the following assumptions: (1) In the cell culture there is a single cell population; (2) cell division times follow Gaussian probability distributions; and (3) the time distribution of the first division round has a mean and standard deviation different from those of the time distributions corresponding to the subsequent division rounds. Thus, the division times are distributed according to

$$P_n(t) = \frac{1}{\sqrt{2\pi d_n^2}} E^{-\frac{1}{2}\left(\frac{t-t_n}{d_n}\right)}, \tag{10a}$$

where

$$t_n = \begin{cases} \tau_o & \text{if } n = 1, \\ \tau & \text{if } n > 1, \end{cases} \quad d_n = \begin{cases} \sigma_o & \text{if } n = 1, \\ \sigma & \text{if } n > 1. \end{cases} \tag{10b}$$

Note that the G–H model considers that cell heterogeneity arises from differences in the time lag before the first round of division with no variability in doubling times for subsequent division rounds. Hence, our specific model is more general than the G–H model because it allows for any value of the variance in secondary division times σ^2. The G–H model is recovered here when $\sigma_0 \gg \sigma$

Under our assumptions, the general formalism is simplified, obtaining the following expression for the probability that a cell have divided at least n times at time t:

$$H_n(t) = \int_0^t \frac{1}{\sqrt{2\pi\sigma_n^2}} E^{-\frac{1}{2}\left(\frac{x-\tau_n}{\sigma_n}\right)^2} \, \mathrm{d}x \tag{11}$$

where $\tau_n = \tau_o + (n-1)\tau$, $\sigma_n = \sqrt{\sigma_o^2 + (n-1)\sigma^2}$.

Such simplification of the formalism follows the properties of Gaussian distributions. Particularly, that the convolution of two Gaussian distributions is also a Gaussian distribution with mean equal to the sum of the means and standard deviation equal to the square root of the sum of the square of the standard deviations in the former distributions.

Substituting then Eq. (11) in Eq. (8) the expression for the precursor frequencies ($w_n(t)$) in this model can be finally obtained. Note that $w_n(t)$ can be expressed in terms of the classical error function and that $w_n(t)$ is only biologically reasonable for $\tau_n > \sigma_n$, since otherwise there is a non-negligible probability of dividing n times in a negative time period.

The four parameters of this model ($\tau_o, \tau, \sigma_o, \sigma$) can be determined by fitting the data sets presented in Section 2.1. Interestingly, the model fits accurately any of the individual distributions for precursor frequencies (not shown), but it bluntly fails to fit the whole kinetic of these distributions (see below).

Following the steps described in Section 2.3 the model is fitted to the experimental data. First, the time evolution of the frequency of non-dividing precursors cells is adjusted, allowing the estimation of parameters τ_o and σ_o. The results of this fitting step are shown in Fig. 1. Clearly only a rough fit of the data is obtained for any of the two data sets, being the major constraint in these fittings the difficulty to accommodate the observations at t=36 h in the context of the whole kinetics. Moreover, strong divergences between the theoretical prediction and the experimental data are also observed when the model is fitted to the whole kinetic data (second step of fitting, see Section 2.3). Fig. 2 shows how the best fit model (dashed lines) misses the trend of the kinetic evolution for the mean and standard deviation of the experimental precursor frequency distributions, for the two data sets studied here. Fig. 3 (dashed lines plus triangles) shows the best fit of this model to several points in the kinetics of the experimental distributions. All the relevant information of these fittings is resumed in Table 3. Noticeably, the χ^2 values obtained are very large, over 200, and the relative error to make the fittings significant are greater that 50%, corroborating the bad quality of the fittings.

The failure of this model to fit the data can be understood in two alternative ways: Either it indicates that division times are not normally distributed or it indicates the existence of more than one cell type in our initial culture. Since there is not clear biological reason to assume the existence of more than one cell population in the experimental data analysed here, we favor in this work the first alternative. In the next section we explore this possibility using in our general model a, bell-shaped, non-Gaussian distribution of division times.

3.3. Alternative model: division time is gamma distributed

An alternative to G–H model is obtained from the general framework assuming the following: (1) there is a single cell population in the culture; (2) the cell division time is Gamma distributed; (3) the parameters of the Gamma distribution differ for the first and the remaining rounds of division, i.e. the distributions will have the same shape parameter (λ) and different localization (a) and scale (b) parameter. Thus, the division times are distributed according to

$$P_n(t) = \begin{cases} 0 & \text{if } t < a_n, \\ \dfrac{1}{b_n \Gamma(\lambda)} \left(\dfrac{t-a_n}{b_n}\right)^{\lambda-1} E^{-\left(\frac{t-a_n}{b_n}\right)} & \text{if } t \geqslant a_n, \end{cases} \tag{12a}$$

where

$$a_n = \begin{cases} \tau_0 & \text{if } n = 1, \\ \tau & \text{if } n > 1, \end{cases} \quad b_n = \begin{cases} b_0 & \text{if } n = 1, \\ b & \text{if } n = 1. \end{cases} \tag{12b}$$

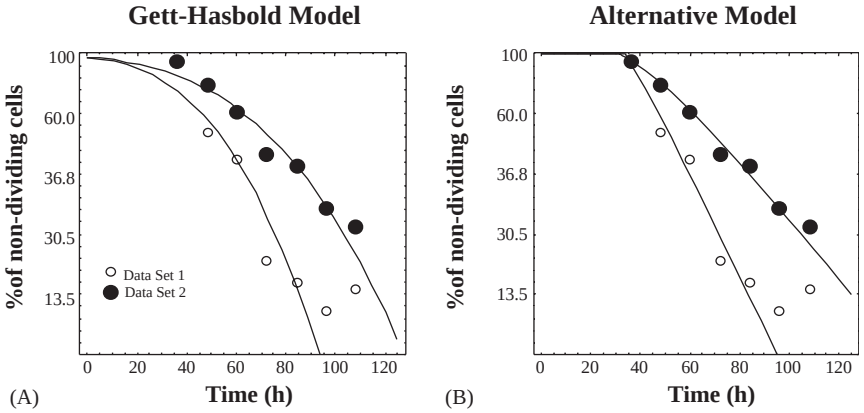

Fig. 1. (A, B) Model fitting to the time evolution of the frequency of non-dividing cells (first fitting step) for models in Sections 3 in the two different data sets studied. The results illustrate how the Hasbold model (Section 3.2) considerably deviate from the experimental data at the initial time points of the kinetics, as situation that is clearly corrected by the alternative model proposed (Section 3.3).

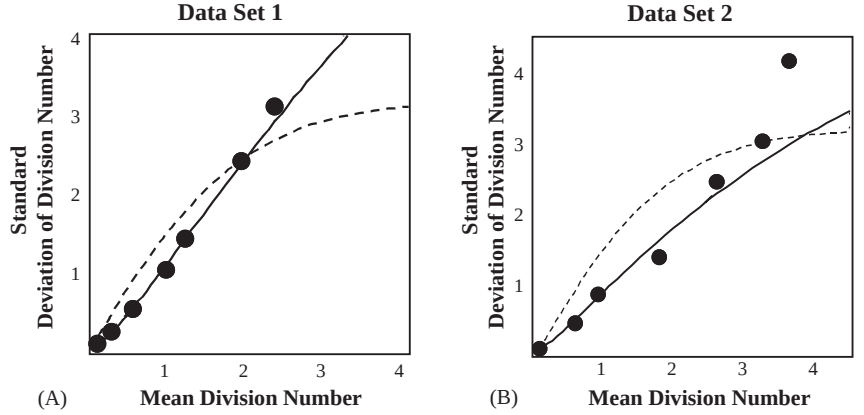

Fig. 2. (A, B) Parametric plot of the kinetic evolution of the mean and the standard deviation of the precursor frequency distribution. The circles correspond to the values obtained experimentally for the indicated data set, while the lines are the values obtained by the models in Section 3 under the best fitting condition. Dashed lines correspond to the Hasbold model and solid line to the alternative model proposed in this work. Only the alternative model follows the experimental trends.

The gamma distribution is a family of distributions where the distribution shape is controlled by parameter λ, the so-called shape parameter. As shown in Fig. 4 for small values of λ the distribution is quite asymmetric (skewed to the left), tending to an exponential as λ tends to 1. As λ increases the distribution becomes more symmetric converging to a Gaussian distribution. Another important property of this distribution is that the convolution of two Gamma distributions with equal scale and localization parameters is a new Gamma distribution with the same scale and whose shape and localization parameters are, respectively, the sums of the shape and localization parameters of the two original distributions. These properties allow reducing to a single Gamma distribution all the secondary rounds of division. Therefore, the probability that a cell have divided at least n times at time t simplifies to

$$H_n(t)=\begin{cases}\dfrac{E^{\left(\frac{\tau_o}{b_o}\right)}}{b_o\Gamma(\lambda)}\displaystyle\int_{\tau_o}^{t}\left(\frac{x-\tau_o}{b_0}\right)^{\lambda-1}E^{-\left(\frac{x}{b_o}\right)}\mathrm{d}x & n=1,\\ \dfrac{E^{\left(\frac{\tau_o}{b_o}+\frac{\tau_n}{b}\right)}}{b_o\Gamma(\lambda)b\Gamma(\lambda_n)}\displaystyle\int_{\tau_o+\tau_n}^{t}\left(\int_{\tau_n}^{x_1-\tau_o}\left(\frac{x_1-x-\tau_o}{b_0}\right)^{\lambda-1}\left(\frac{x-\tau_n}{b}\right)^{\lambda_n-1}E^{-\left(\frac{x1-x}{b_o}+\frac{x}{b}\right)}\mathrm{d}x\right)\mathrm{d}x_1 & n>1,\end{cases}\tag{13}$$

where $\tau_n=(n-1)\tau$, $\lambda_n=(n-1)\lambda$, and Γ is the classical Gamma function.

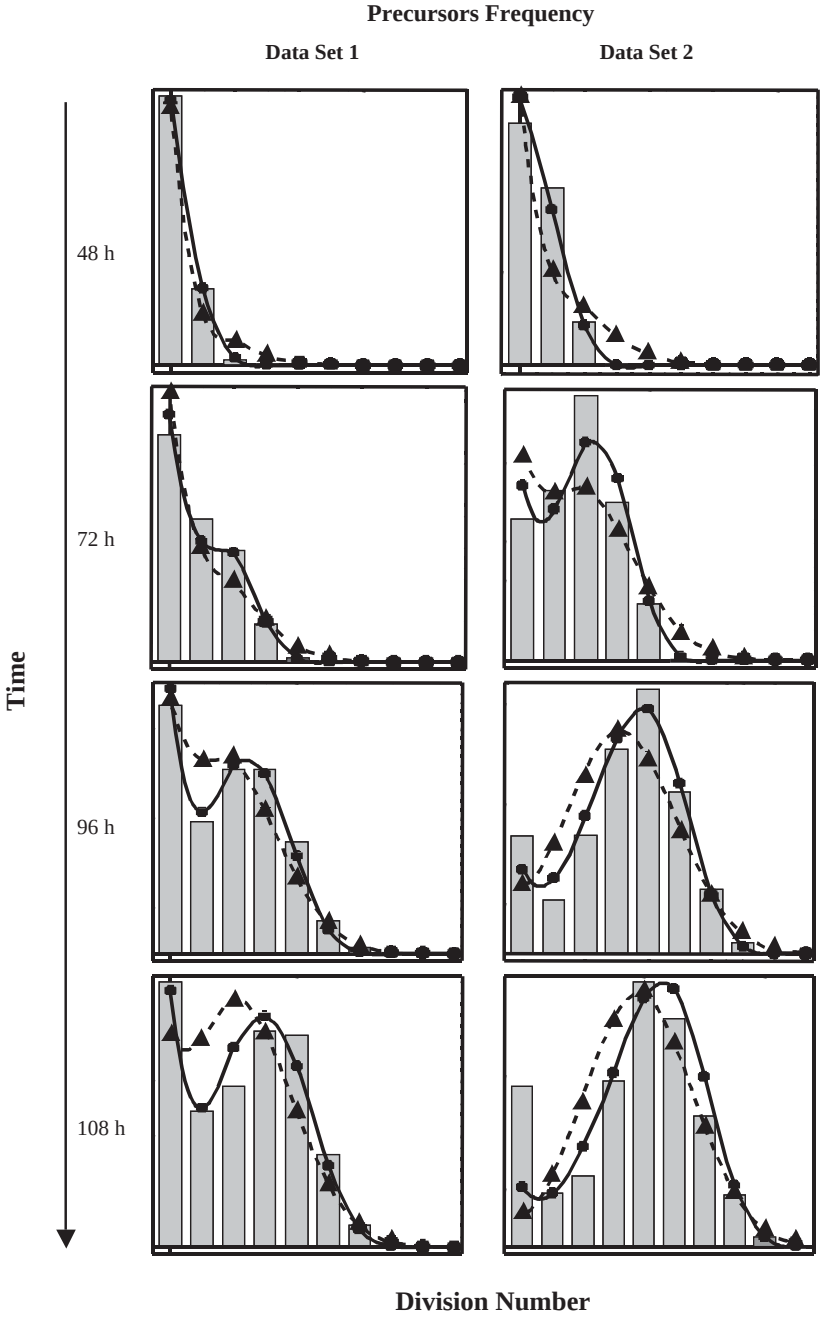

Fig. 3. Detailed fittings of experimental precursors frequencies by the models in Section 3. Four out of seven time points in the kinetic are illustrated here. The gray bar represent the actual experimental value, while the combination of lines + symbol represent the prediction from a theoretical model. Dashed line + triangles are the results for Hasbold model (Section 3.2), and Solid lines + circle are the results for our alternative model (Section 3.3). From the result is clear that our alternative model fit the experimental data much better than the Hasbold model.

The precursor frequencies ($W_n(t)$) are obtained by substituting the Eq. (13) in Eq. (8). This expression is more complicated than the corresponding one in the previous model, but it is still numerically tractable. The five parameters (τ_o, τ, b_o, b, λ) of the model can be determined by fitting to the experimental data in Section 2.2.

The best-fit obtained with this alternative model is much better than the one obtained with the G–H model. This result is shown in Fig. 1 where an obvious improvement in the fittings of the kinetics of non-dividing precursors cells can be observed. Also the global kinetics fittings are greatly improved (solidlines Figs. 2 and 3) with a drastic reduction of the χ^2 values and relative errors as low as 5% for data set 1 and 9% for data set 2, making the fittings significant (Table 3).

Table 3
Best fit parameters models in Section 3

Data #	Parameters	τ_o (h)	σ_o (h)	τ (h)	σ (h)	—	χ^2	Err.
The Hasbold model								
1	Best Fit	73.4	39.1	22.4	10−8	—	244	> 50%
	Confidence Range	(68.0–80.4)	(28.8–43.8)	(18.5–26.7)	(0.0–13.5)	—		
2	Best Fit	53.8	28.5	16.3	10^{-8}	—	406	> 50%
	Confidence Range	(47.6–59.6)	(16.0–33.0)	(13.6–18.5)	(0.0–9.6)	—		
Alternative model								
Data #	Parameters	τ_o (h)	σ_o (h)	τ (h)	b (h)	λ	χ^2	Err.
1	Best Fit	31.6	24.5	8.0	5.3	1.41	31.6	5.0%
	Confidence Range	(30.6–32.5)	(23.6–25.5)	(7.5–8.6)	(4.9–5.6)	(1.37–1.44)		
2	Best Fit	33.9	15.7	7.2	4.3	1.12	52.7	9.0%
	Confidence Range	(33.2–34.6)	(14.8–16.6)	(6.7–7.6)	(4.0–4.6)	(1.10–1.15)		

Using our fitting procedure with the GH models very low values of σ are obtained. However they set the model to operate in a parameter range where it behaves like the Gett and Hasbold model (Gett and Hodgkin, 2000).

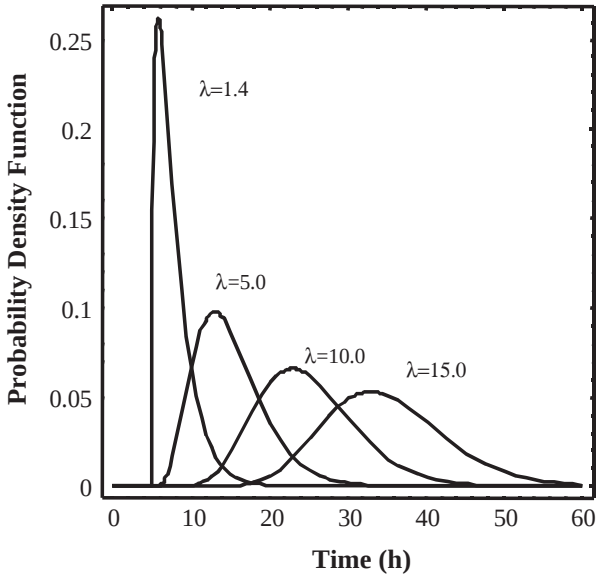

Fig. 4. Dependence of the Gamma probability distribution with the shape parameter λ. In this calculation the remained parameters of the distribution are kept constant and equal to: $b = 2.0$ h, $m = 5.0$ h. The Gamma distribution is quite asymmetric for low values of the parameter λ and become more and more symmetric as λ become larger and larger.

In respect to the estimated parameter values (Table 3) there are several aspects that deserve to be highlighted. First, the values of the shape parameter λ are quite low, i.e. $\lambda = 1.4$ and $\lambda = 1.12$ for data sets 1 and 2, respectively. These values correspond to shapes of the gamma distribution, close to an exponential distribution, and quite distinct from normal distributions. Second, the distribution describing the first round of division is markedly different from the one describing the subsequent division rounds. Such difference becomes evident from the values obtained for the mean ($t_d^n = t_n + \lambda b_n$) and the standard deviation ($Std_n = \sqrt{\lambda}\, b_n$) in the fitted distributions. For instance, for the first division round and for the subsequent division rounds in data set 1 the model predicts $t_1^d \pm Std_1 = 83.5\text{ h} \pm 29.0\text{ h}$ and $t_{n>1}^d \pm Std_{n>1} = 15.4\text{ h} \pm 6.2\text{ h}$ respectively, while in data set 2 the model predicts $t_1^d \pm Std_1 = 59.5\text{ h} \pm 16.6\text{ h}$ and $t_{n>1}^d \pm Std_{n>1} = 12.0\text{ h} \pm 4.5\text{ h}$. This result supports the conclusion of Hasbold et al. (1999) that most of the heterogeneity of cell division is due to the first division round ($Std_1 \gg Std_2$). However, heterogeneity in the second or subsequent division rounds is not at all negligible, contributing significantly to the goodness of the fitting. Actually, fitting the model for $b=0$ leads to fittings with $\chi 2$ values of 50 for data set1 and 101 for data set 2, which are significantly higher than those obtained by letting parameter b free (Table 3).

Further, the values for the mean division times of the T lymphocytes we obtained agree with previous estimations (ranging from 4 to 20 h; Jelley-Gibbs et al., 2000; Lee et al., 2002; Murali-Krishna et al., 1998; Usherwood et al., 1999;

van Stipdonk et al., 2001; Veiga-Fernandes et al., 2000). Also, we confirm previous reports on the existence of a slow initial phase in T cell division followed by a faster one (Iezzi et al., 1998; Jelley-Gibbs et al., 2000; Lee et al., 2002; Usherwood et al., 1999; Veiga-Fernandes et al., 2000).

Last, according to the model the effect of anti-CD28 in the cell culture (compare set 1 vs set 2) is to reduce drastically both the mean and the standard deviation of the division times in all division rounds. Interestingly this effect comes from a major change in only the scale parameter b_n of the gamma distribution. This result suggests, in contrast to the conclusion reported by Hasbold et al. (1999), that the co-stimulation with anti-CD28 mAb affects cell behavior at all division rounds, promoting a faster and more homogeneous cell division as expected from current immunological knowledge.

Noteworthy, the model analysis in this section does not allow estimating the death rate constant of the T cell population (parameter k_d in Eq. (7)) because information on absolute cell numbers is lost when calculating precursor frequency distribution (see Section 2.2). But these models have a simple straightforward prediction that allows estimating the death rate constant from experimental data. Thus, an apparent number of precursors—i.e. the sum of the effective precursor frequencies in all generations multiplied by the absolute number of cells in culture at time t—should decrease exponentially with time. Although information on absolute cell numbers was not available for the particular data set used here (from Fig. 2 of Gett and Hodgkin, 2000). we confirmed this prediction of the models with another data set from the same report (from Fig. 4c), and estimated the average lifespan of the T cells to be 66 h (not shown).

3.4. Specific discussion

The general mathematical framework provided in this section to model the division history in heterogeneous cell populations is based on the assumption that heterogeneous cell division is a consequence of intrinsic noise in the dynamics of cell machinery.

The formalism proposed here is descriptive and relies on defining before hand a set of probability distributions for the doubling time of cells in a given generation. The main question is, thus, how to chose the proper set of probability distributions. In a first instance, following Gett (Gett and Hodgkin, 2000) and Hasbold (Hasbold et al., 1999) proposal, the distributions were set to be Gaussian, but the results of the fitting clearly rule out this possibility (Table 3). In contrast, a generic distribution like the Gamma distribution was instrumental to accurately fit the two experimental data sets studied. Moreover, the values of parameter λ in the gamma distributions recovered in these independent fittings were quite small, corresponding to an extremely asymmetric shape of the (skewed to the left) distribution of cell doubling times, very close to an exponential distribution. This result explains why the Hasbold model is unable to fit the data and indicates that the same type of asymmetric distribution describes these two distinct biological situations. Moreover, the distribution proposed here agrees very well to previous experimental results in many different cell types revealing a normal distribution of cell division rates, and thus an asymmetry distribution in division times (Cantrell and Smith, 1984; Kubitschek, 1970). The latter observation opens the questions on whether a unique type of distribution exists describing heterogeneity in cell division and on what its biological interpretation might be.

Summarizing the analysis performed in this section proposes that heterogeneity in T cell division times, as revealed by typical CFSE assays, can be properly described by an asymmetric Gamma distribution (low value of the shape parameter λ).

4. Modeling the generation-structure of a homogeneous cell population in which cell cycle progression is controled by stochastic interactions with extracellular agents

4.1. A general framework

Lets consider a scenario with a homogeneous cell population where variability of cell-division times derives from stochastic interactions with extracellular agents. Conceptually cell division requires at least two steps: The first one is activation, where the interaction of resting cells with an external stimulus sets on the cellular machinery for division. The second step is cell cycle progression, where the activated cells execute an intrinsic cellular program that leads after sometime to cell division. The resulting daughter cells either revert to a resting state (requiring further activation for reentering the cell cycle) or reenter immediately into cell cycle, undergoing a second division round (without requiring further activation). To model this scheme we define two compartments A and B. The compartment A comprises all resting cells in the culture, while the compartment B comprises all activated cells. The activation process (transition of A to B) is modeled as a first-order kinetic process, accounting in a simple way for the stochastic components in cell interaction. On the other hand, the compartment B is modeled as deterministic with a fixed characteristic transition

time. After each division round, daughter cells are assumed to have a constant probability α of returning to compartment A and the complementary probability $1-\alpha$ to stay in compartment B starting a new division cycle. The model equations are as follows:

$$\frac{da_n(t)}{dt} = -r_n a_n(t) + 2\alpha\kappa_{n-1} b_{n-1}(t, L) - d_n a_n(t), \tag{14a}$$

$$\frac{db_n(t,x)}{dt} = -\kappa_n \frac{\partial b_n(t,x)}{\partial x}, \tag{14b}$$

$$b_n(t,0) = r_n a_n(t)\kappa_n + 2(1-\alpha)\kappa_{n-1} b_{n-1}(t,L)/\kappa_n, \tag{14c}$$

where t is the time, x the cell cycle position of activated cells. It ranges from 0 to L, n the number of divisions undergone by a given cell (generation number), α the probability of reverting to resting state after division, $a_n(t)$ the number of resting cells in generation n at time t. For coherence in the formulation it is set to 0 if $n<0$, $b_n(t,x)$ the number of activated cells which are in generation n at time t and at cell cycle position x. For coherence in the formulation it is set to 0 if $n<0$, r_n the activation rate for cells in generation n, d_n the exponential death rate constant of resting cells in generation n, κ_n the cell cycle progression rate of activated cell in generation n.

Eqs. (14a) and (14b) describe the dynamics of compartments A and B, respectively, while Eq. (14c) is a boundary condition for the transition between compartments.

To analyse the experimental data, Eq. (14) has to be solved using as initial conditions that all cells belong to the resting state of generation zero at $t=0$. In this case the expected precursor frequency distribution is obtained as

$$w_n(t) = \frac{(a_n(t) + b_n^t(t))}{2^n} \Bigg/ \sum_{k=0}^{\infty} \frac{(a_k(t) + b_k^t(t))}{2^k}, \tag{15}$$

where, $b_n^t(t) = \int_0^L b_n(t,x)\,dx$ is the total number of cells in compartment B belonging to generation n.

Eq. (14) can be solved applying the Laplace transform (Spiegel and Liu, 1999) to the temporal dimension obtaining

$$sA_n(s) - a_n(0) = -r_n A_n(s) + 2\alpha\kappa_{n-1} B_{n-1}(s,L) - d_n A_n(s), \tag{16a}$$

$$sB_n(s,x) - b_n(0,x) = -\kappa_n \frac{\partial BL_n(s,x)}{\partial x}, \tag{16b}$$

$$B_n(s,0) = r_n A_n(s)/\kappa_n + 2(1-\alpha)\kappa_{n-1} B_{n-1}(s,L)/\kappa_n, \tag{16c}$$

where capital letter symbols stand for the Laplace transform of the corresponding lower case function and s is the variable that substitutes time upon the Transformation. Given the above initial conditions (i.e., $b_n(0,x)=0$ for any value of x) Eq. (16b) is solved as

$$B_n(s,x) = B_n(s,0)E^{-s\cdot x/\kappa_n}, \tag{17a}$$

which is used to transform the boundary condition (16c) into (see Appendix A)

$$B_n(s,0) = \sum_{k=0}^{n} (2(1-\alpha))^k (r_{n-k}/\kappa_n) A_{n-k}(s) E^{-s\sum_{1=n-k}^{n-1} L/\kappa_1} \tag{17b}$$

Substituting now Eq. (17b) in Eq. (16a), and after some algebraic manipulation, it yields

$$A_n(s) = \begin{cases} a_0(0)/(s+(r_0+d_0)) & \text{if } n=0 \\ \dfrac{2^n \alpha r_0}{s+(r_n+d_n)} \left(\prod_{k=1}^{n-1} \left(\dfrac{\alpha r_k}{s+(r_k+d_k)} + (1-\alpha) \right) \right) E^{-s\sum_{k=0}^{n-1}\tau_k} A_o(s) & \text{if } n>0, \end{cases} \tag{18a}$$

$$B_n(s,x) = 2^n \frac{r_0}{\kappa_n} \left(\prod_{k=1}^{n-1} \left(\frac{\alpha r_k}{s+(r_k+d_k)} + (1-\alpha) \right) \right) E^{-s\left(\sum_{k=0}^{n-1}\tau_k + x/\kappa_n\right)} A_0(s), \tag{18b}$$

where $\tau_n = L/\kappa_n$ is the cell cycle time for cells in generation n.

Finally, an analytic expression for $a_n(t)$ and $b_n(t,x)$ is obtained by taking the Inverse Laplace Transform of Eq. (18). Substituting those expressions into Eq. (15) provide explicit solutions for the precursor frequency distributions.

In this general model every parameter involved in cell dynamics is potentially dependent on cell division history (subindex n), and consequently the model can have an infinite number of parameters (τ_n, r_n, d_n). In order to handle it,

and particularly to relate it to experimental data, explicit dependencies on the generation index n have to be assumed for each parameter. Two particular realizations of this model are studied in the next two subsections.

4.2. Modified Nordon model: activation time independent of division history

A simple extension of the Nordon (N) model is recovered from the above general formalism by making the following three assumptions. (1) The activation rates and the decay rates of cells are independent of the generation number, i.e. r_n=r and d_n=d, for $n \geqslant 0$. (2) The cell cycle time in the first division round is bigger than the one on the subsequent division rounds $\tau_0 > \tau_{(n>0>} = \tau$. (3) After, each division the resulting daughter cells revert to the resting state $\alpha = 1$. In this case the model has the following the solution (see Appendix B)

$$a_n(t) = \begin{cases} a_0(0)E^{-qt} & \text{if } n = 0, \\ \dfrac{a_0(0)(2r)^n}{n!}\vartheta[t-(n-1)\tau-\tau_0]^n E^{-q(t-(n-1)\tau-\tau_0)} & \text{if } n > 0, \end{cases}$$

$$b_n^t(t) = \begin{cases} a_0(0)\dfrac{r}{q}\{E^{-q\vartheta[t-\tau_0]} - E^{-qt}\} & \text{if } n = 0, \\ a_0(0)2^n r^{n+1}\left\{\dfrac{\Gamma(n+1,\ q\vartheta[t-n\tau-\tau_0]) - \Gamma(n+1,\ q\vartheta[t-(n-1)\tau-\tau_0])}{n!q^{n+1}}\right\} & \text{if } n > 0, \end{cases} \tag{19}$$

where $\Gamma(n,x)$ is the Gamma function, $q = r + d$ and ϑ is defined as

$$\vartheta[x] = \begin{cases} 0 & \text{if } x < 0, \\ x & \text{if } x \geqslant 0. \end{cases} \tag{20}$$

Note that although the cell cycle time for the first round of division is explicitly modeled here as different (bigger) than the cell cycle times at any subsequent round of division, this is equivalent to assume a lag time (equal to $\tau_0 - \tau$) at the beginning of the culture. Note that the original Nordon model is obtained from this modified version by setting $\tau_0 = \tau$.

This model has four parameters (τ_0, τ, r and d) that can be estimated by fitting the model to the experimental data. To facilitate parameters comparison with previous models, we will refer systematically here to the mean activation time (t_a) and mean lifespan and (t_d) instead of the former activation and death rate constants. Note that by definition $r = 1/t_a$ and $d = 1/t_d$.

This model fits accurately any individual precursor frequency distributions in the experimental data sets (data not shown), but it fails to explain the whole kinetic process, as assessed with our two-step fitting procedure.

Fitting the time evolution of the fraction of undivided cells (first fitting step), the parameters τ_0, t_a and t_d are initially estimated (Fig. 5). Interestingly, for the two data sets used here, the model predicts that that fraction decays exponentially with a very large value of the life span ($t_d \to$) and with an explicit initial time delay. As shown in Fig. 5 the predicted dependency agrees very well with the experimental data set #1, while for data set #2 all the time points except the last one ($t = 108$ h) are fitted reasonably well by the model.

The results of the second fitting step are shown in Figs. 6 (dashed lines) and 7 (dashed lines plus solid triangle). Although this model does not predict properly the time evolution of the mean and standard deviation of the precursor frequency distribution observed in data set #1, apparently it predicts it reasonable well for data set #2 (Fig. 6). However, a detailed analysis of the fitting shows (Fig. 7, dashed lines plus triangles) a clear discrepancy between the model prediction and the experimental data for both data sets. The failure of the model to explain the data is reflected in the remarkably high χ^2 values obtained (Table 4) and the requirement of an experimental error greater than 50% to make the fittings significant.

The failure of this model to explain the full kinetic evolution (fitting step 2) in both experimental sets is quite striking, given that the model fits well the kinetic evolution of the undivided cells in the cultures (fitting step 1). However, the values for τ_0 and t_a obtained as best fit parameters in the fitting step 2 are very different from their initial values obtained from fitting step 1 (compare parameter in Fig. 5 to those on Table 4). This fact illustrates that the model is structurally constrained in a way that it is unable to make compatible the time evolution of the undivided cells with the time evolution of cells that have undergone several rounds of division. In the following section the model is extended in order to overcome this problem.

4.3. The extended model: activation time is dependent on the division history

The previous model is extended here by relaxing the assumption of an equal activation time at any cell generation. Inspired by the results of Section 3, we assume that the activation rate in the first round of division is different from the

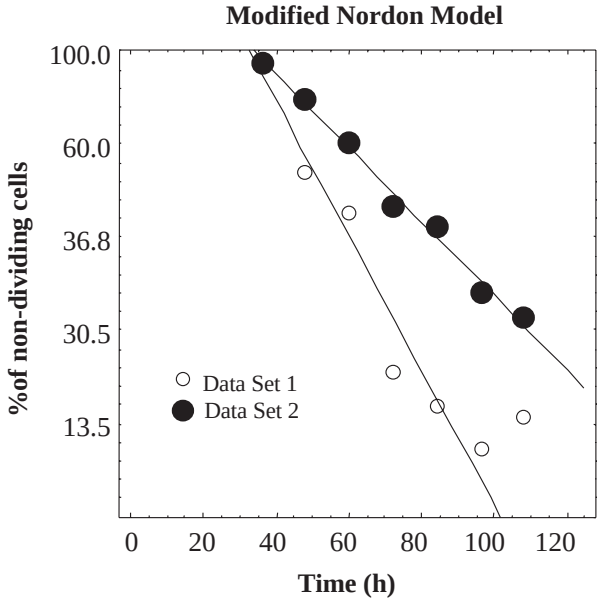

Fig 5. Results of fitting the time evolution of the frequency of nondividing cells (first fitting step) for the Nordon model models (Sections 4.2), in the two different data sets studied. The results illustrate how the model fit considerably well the experimental data excluding the last kinetic point in data set 2.

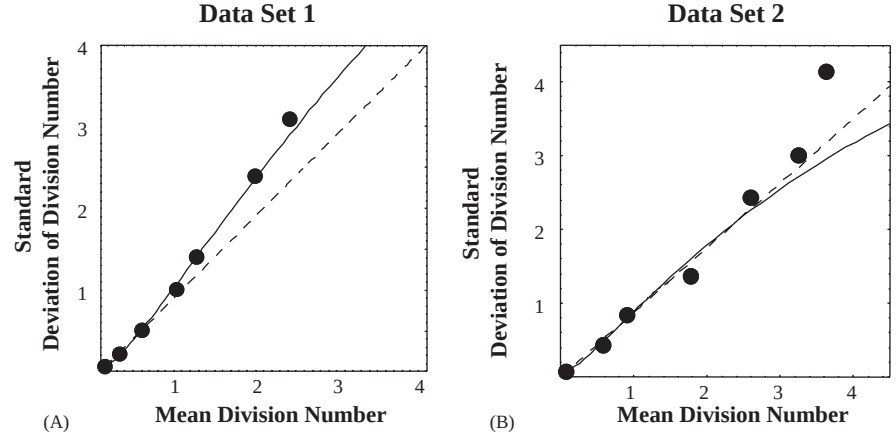

Fig 6. (A, B) Parametric plot of the kinetic evolution of the Mean and the Standard deviation of the precursor frequency distribution. The circles correspond to the values obtained experimentally for the indicated data set, while the lines are the values obtained by the models in Section 4 under the best fitting condition. Dashed lines correspond to the Nordon model and solid lines to the extended model proposed in this work. Both models follow the experimental trends for data set 2 (excepting the last kinetic point). However, for data set 1 the Nordon model fails to explain the data, while the extended model accurately follows the experimental trend.

one in subsequent division rounds $r_0 \neq r_{(n>0)} = r$. In this case the solution of the model is (see Appendix C):

$$a_n(t) = \begin{cases} a_0(0)E^{-qt} & \text{if } n = 0, \\ a_0(0)(2r)^n r_0 \left\{ \dfrac{\Gamma(n) - \Gamma(n,(q-q_0)\vartheta[t-(n-1)\tau-\tau_0])}{\Gamma(n)(q-q_0)^n r} \right\} E^{-q_0\vartheta(t-(n-1)\tau-\tau_0)} & \text{if } n > 0, \end{cases}$$

$$b_n^t(t) = \begin{cases} a_0(0)\dfrac{r_0}{q}\{E^{-q_0\vartheta[t-\tau_0]} - E^{-q_0 t}\} & \text{if } n = 0, \\ a_0(0)r_0(2r)^n \left\{ \dfrac{\Gamma(n+1,\ q\vartheta[t-n\tau-\tau_0]) - \Gamma(n+1,\ q\vartheta[t-(n-1)\tau-\tau_0])}{n!q_0 q^n} \right\} & \\ \qquad + \dfrac{(q_0-q)}{2q_0}\{a_{N+1}(t+\tau) - a_{n+1}(t)\} & \text{if } n > 0, \end{cases} \tag{21}$$

where functions and parameters have the same meaning as in the previous section.

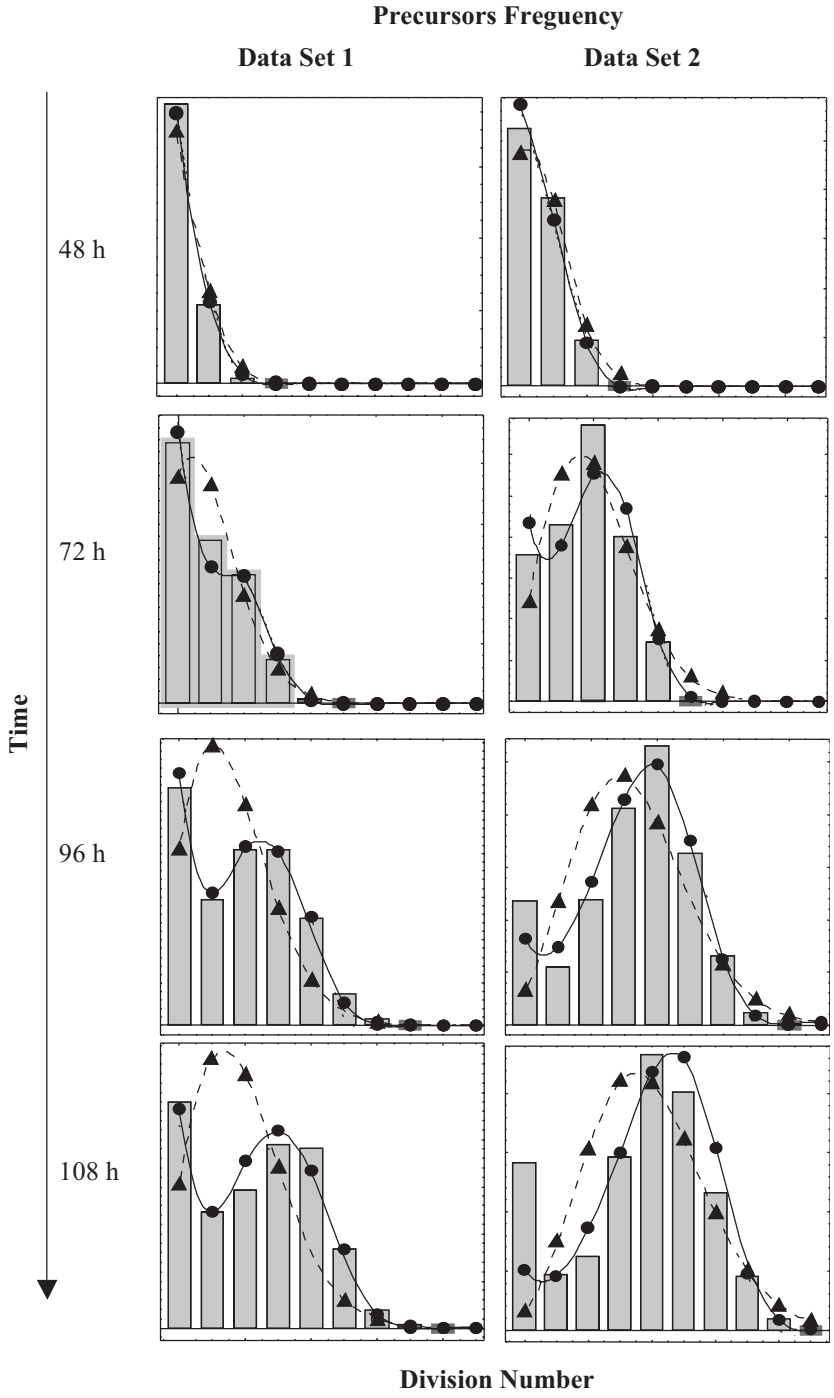

Fig 7. Detailed fittings of experimental precursor frequencies by the models in Section 4. Four out of seven time points in the kinetics are illustrated here. Gray bars represent actual experimental values, while the combinations of lines + symbol represent the prediction from theoretical models. Dashed lines + triangles correspond to the Nordon model (Section 4.2), and solid lines + circles correspond to the extended model Section 4.3.

The results of the fitting of the time evolution of undivided cells with this extended model are identical to those with the modified Nordon model (Fig. 5). Consequently, the model is able to explain very well the data (except for $t = 108$ h in data set #2) in this first fitting step. On the other hand, introducing this difference in the activation times considerably improves the capacity of the model to fit the full kinetics in the two data sets. Fig. 6 (solid lines) shows that this model describes reasonably well the time evolution of the mean and standard deviation of precursor frequency distributions in both experimental data sets (except the last time point in data set #2). Moreover, the detailed fitting of the experimental distributions by this second model is significantly improved for each individual time point (Fig. 7,

Table 4
Best fit parameters for models in Section 4

Data #	Parameters	t^a(h)	τ_0(h)		τ (h)	t^d(h)	χ^2	Err.
The modified nordon model								
1	Best fit	27.2	33.7	—	0.01	∞	484	> 50%
	Confidence range	(21.4–36.2)	(31.8–40.5)	—	(0.0–2.2)	0–∞)		
2	Best fit	12.3	34.7	—	1.2	∞	298	> 50%
	Confidence range	(10.9–14.2)	(34.0–35.9)	—	(0.01–3.4)	(0–∞)		
The extended model								
Data #	Parameters	t^a(h)	—	τ (h)	t^d(h)	χ^2	Err.	
1	Best Fit	36.1	33.8	8.4	8.5	299	32.0	5.1%
	Confidence range	(34.8–37.5)	(33.0–34.7)	(7.9–9.1)	(7.9–0.9.1)	(122–∞)		
2	Best Fit	17.6	34.2	5.4	6.8	297	54.9	9.3%
	Confidence range	(16.9–18.4)	(33.6–34.9)	(5.07–5.8)	(6.3–7.2)	(68–∞)		

solid lines plus circles). This is reflected in the reduction of the χ^2 values obtained (Table 4) and in a drastic reduction of the relative errors that make significant the fitting (5.1% for data set #1 and 9.3% for data set #2).

Several aspects in these fittings are noteworthy. First, the reduction in the activation time from the first round of division to the subsequent division rounds (a factor 4.5 for the data set #1 and a factor 3.3 for the data set #2) appears essential for the quality of the fitting (see next subsection).

Second, the values for the mean lifespan estimated by the model are large as compared to estimates from in vitro T lymphocyte cultures. Nevertheless, the fitting of the model is insensitive to these values (note the large confidence intervals in Table 4). The insensitivity to the value of the death rate constant stems from the previously acknowledged fact that information on absolute cell numbers is lost in the calculation of effective precursor fequencies. As discussed in the end of Section 3.3, an accurate estimation of this parameter requires fitting of apparent precursor numbers at time t. We fitted this model to the apparent precursors cell numbers at three consecutive times obtained from Fig. 4c in Gett and Hodgkin (2000). We obtained a good fitting and estimated the T cell life span to be about 39 h (not shown).

On the other hand, the estimates of the mean division times (i.e., cell cycle time + mean activation time divided by ln(2)) are quite reasonable for data set #1 ($t_0^a/\ln(2)+\tau_0) = 69.6$ h and ($t^a/\ln(2)+\tau) = 17.0$ h, as well as, for data set #2 ($t_0^a/\ln(2)+\tau_0) = 51.6$ h and ($t^a/\ln(2)+\tau) = 12.1$ h, matching very well the estimates in Section 3.2. Therefore, according to the discussion in Section 3.3, these are biologically reasonable estimates. Finally, a comparison of the estimated parameters for data set #1 and #2 suggests that the addition of anti-CD28 antibodies in the cell cultures affects mainly the mean activation times, reducing them in all division rounds. This result is compatible with the classical understanding for the role of co-stimulation in T cell physiology.

4.4. Specific discussion

The modeling framework presented in this section is based on the assumption that asynchrony in cell division is caused by the stochastic character of cell interactions. In the general formalism it is assumed that the value of several parameters (namely d_n, τ_n and k_n) may vary with cell division history. In some particular realizations this formalism leads to analytic formulas for the quantitative analysis of the results of CFSE experiments. Two of these particular realizations were explicitly studied here. In the first one, the formalism was reduced to the model proposed by Nordon et al. (1999). The results showed that this model is unable to fit the experimental data analysed here. The second realization of the formalism is an extension of the first one derived by assuming an explicit dependence of the activation times with cell division history. This extended model correctly fit the experimental data, predicting that cell activation time in the first division round is 3–4 fold bigger than cell activation times at subsequent divisions.

Such dependency of activation times with cell division history might result from a cooperative effect in the cell population that correlates in time with the mean cell behavior. For instance, entry into cell cycle depends on autocrine/paracrine factors, such as IL-2, that are produced by the T cells themselves. Therefore, effective activation times may decrease as the number of activated cells increases in time leading to a cooperative accumulation of autocrine/paracrine factors. This interpretation of our results is, however, minimized by the fact that the cultures under study were supplemented with exogenous IL-2 (Gett and Hodgkin, 2000).

Alternatively the results in this section, can be interpreted as indicating, that once T cells are activated they acquire some properties, allowing them to progress faster into cell cycle than naïve cells. This is a property that has been often claimed as distinctive of memory T cells (Dutton et al., 1998; Iezzi et al., 1998; Swain et al., 1996). During T cell activation and division several molecules are known to be up regulated and may remain upregulated in the daughter cells. Some of these molecules may facilitate further activation and progression into cell cycle. A good example is CD25, a subunit of the high affinity receptor of IL-2, which is up-regulated upon T cell activation and controls cell cycle progression (Cantrell and Smith, 1984).

Yet another interpretation of our results is that T cells, once activated, could undergo several division rounds in an antigen-independent fashion. Clearly such antigen-independent proliferation will resemble an apparent activation time much lower in secondary division rounds than in the first division round. However, while this phenomenon has been well documented for CD8+ T cells (van Stipdonk et al., 2001) it is much less supported for CD4+ T cells (Jelley-Gibbs et al., 2000; Lee et al., 2002). Nevertheless, the general model presented here can already account for this type of behavior by simply setting $0<\alpha<1$, which leads to a complex but analytic solution (not shown).

5. General discussion

This paper provides several mathematical models to analyse experiments of cell proliferation using CFSE labeled cells. The models are classified in two classes according to the proposed causes for the observed asynchrony in cell division. The first class of models (Section 3) assumed that asynchronous division was based on a purely intrinsic heterogeneity of cell populations, while the second class of models (Section 4) assumed that it resulted from the stochastic nature of the interactions of a cell with its surroundings. Two general mathematical frameworks were developed for each of these explanations and a particular model in each class was found that explains reasonably well the experimental data analysed here.

The best model in each class accounts equivalently well for the experimental data. The minimum χ^2 values obtained are comparable in both models, which have a similar number of parameters. Further, based on the estimated physiological parameter values the two best models predict similar cell behaviour in the analysed experimental conditions. For instance, they predict similar mean division times, they show a difference in T-cell proliferation kinetics between the initial division round and the subsequent ones, and they show an accelerated division kinetics in any division round induced by co-stimulation with anti-CD28 antibodies. In summary, the best models in each class take relevant biological conclusions out of the analysed data. But what does the study of these two classes of models tell us about the cause of asynchronous cell division? To approach this question let's look closer to each set of the proposed models.

The models in the first class are descriptive, and their basic assumption is the possibility of finding a set of probability distributions for the division time of cells in different generations that accurately describe the observed cell behavior. Note that although the most straightforward interpretation of those models is that they strictly describe intrinsic cell heterogeneity, those distributions could be very well capturing many other phenomena, including cell interactions. It is easy to realize that this first group of models can reproduce the behavior of models in the second group by setting $\lambda = 1$, $b_o = t_o^a$, $b = t^a$, and keeping the parameters τ_0 and τ with the same meaning in both models. Therefore, in those models the distributions we found are not necessarily related to intrinsic cell heterogeneity. What this analysis suggests is that whatever the cause of heterogeneity in cell division is, it should explain how the observed distribution arises. That is, to substantiate our original hypothesis in this class of models one should develop explicit models of the internal cell machinery for T cell activation and proliferation. Furthermore, one should show that a distribution of internal cell states, such as the asymmetric gamma distribution reported here, could be obtained for instance through the dynamic propagation of some stochastic process in cell machinery. The results of the present study allow ruling out potential causes of asynchronous T cell division. Take for instance the proposal by Cantrell et al (Cantrell & Smith, 1984) that asynchronous T cells division is the result of the heterogeneous expression of CD25 at the T cell surface. In this case CD25 was found to be log-normal distributed, a distribution that although asymmetric is much less skewed to the left than the Gamma distributions reported here. This indicates that, although CD25 density on cell surface may contribute to the asynchrony in cell division, it cannot be the only basis for it.

The second class of models proposed here is a generalization of the classical models for 'activation + cell cycle progression' (Burns and Tannock, 1970; Smith & Martin, 1974), which include generation structure explicitly. The main assumption in this class of models is the existence of a stochastic transition event in cell division, which is described as a Poisson process with a constant transition probability. Such stochastic event was motivated by considering cell interactions, for instance the transition from the non-activated cell to the activated cell dependent on interaction with antigen. However, this transition may as well relate to an internal transition on the cellular machinery

state, which distributes the cell population into two different states. Thus, although this model was inspired on the cell interaction hypothesis it does not rely on it, being general enough to be compatible with both hypotheses. Interestingly, this common way of modeling cell proliferation has proved useful as a mean field model by describing accurately the time evolution of mean quantities in the cell population (for instance, mean population size, mean doubling time, etc.). What is remarkable in our results here is that this type of formalism indeed accounts also for the variances in cell doubling times, as demonstrated by the fact that it accurately fits CFSE results. Thus, our findings strongly suggest the existence of a key transitional event that contributes to the asynchronous cell division. The obvious question is then, what does this transition actually relate to? A possible answer comes from the fact that our model has a richer structure than the aspects on which we focus in our analysis. Note that the models in this second class not only predict how many cells are in generation n at time t, but they also predict the fraction of them that are resting (compartment A) and activated (compartment B), i.e., the proportions that have underwent or not the critical transition. Therefore, by combining CFSE labeling with other classic flow cytometry assay of the cell cycle phase of individual cells (e.g. BrDU labeling) one could assess when the transition event is taking place. If the predicted transition would coincide with some of the known cell cycle check-points (Lodish et al., 1995), in which the T cell is waiting for some external signal to proceed, then one could safely conclude that stochastic cell interactions are the main cause of the heterogeneous cell division. Otherwise, one must conclude that there is a key contribution from intrinsic noise of the internal cellular machinery.

In summary, although the present analysis could not distinguish between the two alternative hypotheses for the cause of asynchronous cell division, it provides some insights into this problem and suggests new ways of combining theoretical and experimental work to quantitatively address and eventually resolve it. Until this controversy is appropriately tackled one may nevertheless ask which class of models should be adopted for more practical issues. In this sense the best model in the first class is simpler and has a fair descriptive power. In our view, this model is the proper choice when one is interested in quantifying heterogeneity in cell division times and its dependence on cell generations, without paying special attention to the causes of such heterogeneity. The descriptive information extracted from data using this approach is limited but valid independently of the underlying mechanism. If, however, one is interested in analysing how a cell interaction mechanism affects cell cycle, or interested in using cell cycle analysis to get insights into an interaction mechanism, then the best model in the second class is the right choice. In this mechanistic model the parameters have a straightforward biological meaning, and the estimated values can be used for hypothesis testing.

Finally, it is worth noting that the best models, in each class, still deviate somewhat from the experimental data. While this may reflect some limitation of the models we developed here, it is important to realize that errors may also have been introduced when the original CFSE-intensity histograms were processed to obtain the data in terms of frequency of cells per generation. Variable CFSE-labeling of the cells, relative importance of autofluorescence, and uneven partition of the CFSE during cell division may generate significant overlaps of the peaks corresponding to each generation in the CFSE-intensity histograms. This can make it difficult to assign cells to the different generations. Deconvolution procedures are currently available that deal with the problem of assigning cells to generations in a way that is independent of the mechanism of cell division. It would be of practical interest to couple the presently proposed mechanistic models for the evolution of the generation-frequency distribution to algorithms that deconvolute the original CFSE-intensity distributions. Fitting of these models, incorporating both mechanism and signal-processing parts, would allow to identify and to quantify the errors of different sources.

Acknowledgements

We are grateful to Dr. Rolando Bizcay from the Faculty of Mathematics of the University of Havana for useful discussions that helped to improve this work. The work was supported by Foundation for Science and Tecnology (Portugal): fellowships to KL and JF (respectively BPD/11575/2002 and BCC/18972/98) and grants to JC (PRAXIS/P/BIA/10094/1998 and POCTI/MGI/46477/2002 with FEDER funds) and JF (POCTI/36413/1999).

Appendix A. algebraic derivation of Eq. (17b), (18a) and (18b)

The first step in deriving Eq. (17b) is to substitute Eq. (17a) in Eq. (16c), which leads to

$$B_n(s,0) = r_n A_n(s)/\kappa_n + 2(1-\alpha)\kappa_{n-1} B_{n-1}(s,0) E^{-s\frac{L}{\kappa_{n-1}}}/\kappa_n.$$

Using the later expression recursively to obtain the values of B_n(s,0) for $n = 0, 1, 2, 3$, results in

$$
\begin{aligned}
B_0(s,0) &= r_0 A_0(s)/\kappa_0,\\
B_1(s,0) &= r_1 A_1(s)/\kappa_1 + 2(1-\alpha) r_0 A_0(s) E^{-s\frac{L}{\kappa_0}}/\kappa_1,\\
B_2(s,0) &= r_2 A_2(s)/\kappa_2 + \left(2(1-\alpha) r_1 A_1(s) E^{-s\left(\frac{L}{\kappa_1}\right)} + (2(1-\alpha))^2 r_0 A_0(s) E^{-s\left(\frac{L}{\kappa_0}+\frac{L}{\kappa_1}\right)}\right) \Big/ \kappa_2\\
B_3(s,0) &= r_3 A_3(s)/\kappa_3 + \left(2(1-\alpha) r_2 A_2(s) E^{-s\left(\frac{L}{\kappa_2}\right)} + (2(1-\alpha))^2 r_1 A_0(s) E^{-s\left(\frac{L}{\kappa_0}+\frac{L}{\kappa_1}+\frac{L}{\kappa_2}\right)}\right) \Big/ \kappa_3,\\
&\vdots
\end{aligned}
$$

By induction, the nth expression in this recursion is

$$B_n(s,0) = \sum_{k=0}^{n} (2(1-\alpha))^k (r_{n-k}/\kappa_n) A_{n-k}(s)\, \mathrm{e}^{-s\sum_{1=n-k}^{n-1} L/\kappa_1}$$

Eq. (18a) is obtained by rewriting Eq. (16a) as:

$$A_n(s) = (a_n(0) + 2\alpha\kappa_{n-1} B_{n-1}(s,L))/(s+q_n),$$

where

$$q_n = r_n + d_0 \quad \text{and} \quad a_n(0)\begin{cases} > 0 & \text{for } n = 0,\\ = 0 & \text{for } n > 0. \end{cases}$$

The latter equations represent the initial conditions of the culture, where all the cells are in generation 0 at $t = 0$.

Substituting Eq. (17b) in the latter expression for $n = 0, 1, 2, 3$ yields

$$
\begin{aligned}
A_0(s) &= a_0(0)/(s+q_0),\\
A_1(s) &= \frac{2\alpha\kappa_0}{(s+q_1)}(B_0(s,0)E^{-s\frac{L}{\kappa_0}})\\
&= \frac{2\alpha r_0}{(s+q_1)} A_0(s) E^{-s\frac{L}{\kappa_0}},\\
A_2(s) &= \frac{2\alpha\kappa_1}{(s+q_2)}(B_1(s,0)E^{-s\frac{L}{\kappa_1}})\\
&= \frac{2\alpha}{(s+q_2)}\left(r_1\frac{2\alpha r_0}{(s+q_1)} A_0(s) E^{-s\frac{L}{\kappa_0}} + 2(1-\alpha) r_0 A_0(s) E^{-s\frac{L}{\kappa_0}}\right) E^{-s\frac{L}{\kappa_1}}\\
&= \frac{4\alpha r_0}{(s+q_2)}\left(\frac{\alpha r_1}{(s+q_1)} + (1-\alpha)\right) A_0(s) E^{-s\left(\frac{L}{\kappa_0}+\frac{L}{\kappa_1}\right)},
\end{aligned}
$$

$$
\begin{aligned}
A_3(s) &= \frac{2\alpha\kappa_2}{(s+q_3)}(B_2(s,0)E^{-s\frac{L}{\kappa_2}})\\
&= \frac{2\alpha}{(s+q_3)}\left(r_2 A_2(s) + 2(1-\alpha) r_1 A_1(s) E^{-s\left(\frac{L}{\kappa_1}\right)} + (2(1-\alpha))^2 r_0 A_0(s) E^{-s\left(\frac{L\,L}{\kappa_0\kappa 1}\right)}\right) E^{-s\frac{L}{\kappa_1}}\\
&= \frac{2\alpha}{(s+q_3)}\left(r_2\frac{4\alpha r_0}{(s+q_2)}\left(\frac{\alpha r_1}{(s+q_1)} + (1-\alpha)\right) A_0(s) E^{-s\left(\frac{L}{\kappa_0}+\frac{L}{\kappa_1}\right)}\right.\\
&\quad \left. + 2(1-\alpha) r_1\frac{2\alpha r_0}{(s+q_1)} A_0(s) E^{-s\left(\frac{L}{\kappa_1}\right)} + (2(1-\alpha))^2 r_0 A_0(s) E^{-s\left(\frac{L\,L}{\kappa_0\kappa 1}\right)}\right) E^{-s\frac{L}{\kappa_2}}
\end{aligned}
$$

$$
\begin{aligned}
&= \frac{2\alpha}{(s+q_3)}\left(r_2\frac{4\alpha r_0}{(s+q_2)}\left(\frac{\alpha r_1}{(s+q_1)}+(1-\alpha)\right)+2(1-\alpha)r_1\frac{2\alpha r_0}{(s+q_1)}(2(1-\alpha))^2 r_0\right)A_0(s)E^{-s\left(\frac{L}{\kappa_0}+\frac{L}{\kappa_1}+\frac{L}{\kappa_2}\right)}\\
&= \frac{2\alpha}{(s+q_3)}\left(r_2\frac{4\alpha r_0}{(s+q_2)}\left(\frac{\alpha r_1}{(s+q_1)}+(1-\alpha)\right)+4(1-\alpha)r_0\left(\frac{\alpha r_1}{(s+q_1)}+(1-\alpha)\right)\right)A_0(s)E^{-s\left(\frac{L}{\kappa_0}+\frac{L}{\kappa_1}+\frac{L}{\kappa_2}\right)}\\
&= \frac{8\alpha r_0}{(s+q_3)}\left(\frac{\alpha r_1}{(s+q_1)}+(1-\alpha)\right)\left(\frac{\alpha r_1}{(s+q_1)}+(1-\alpha)\right)A_0(s)E^{-s\left(\frac{L}{\kappa_0}+\frac{L}{\kappa_1}+\frac{L}{\kappa_2}\right)}\\
&\ \ \vdots
\end{aligned}
$$

By induction the nth expression is this recursion is

$$
A_n(s)=\begin{cases} a_0(0)/(s+(r_0+d_0)) & \text{if } n=0,\\ \dfrac{2^n\alpha r_0}{s+(r_n+d_n)}\left(\prod_{k=1}^{n-1}\left(\dfrac{\alpha r_k}{s+(r_k+d_k)}+(1-\alpha)\right)\right)\mathrm{e}^{-s\sum_{k=0}^{n-1}\tau_k}A_0(s) & \text{if } n>0.\end{cases}
$$

Finally to obtain Eq. (18b) starting from Eq. (18a) we first rewrite the Eq. (16a) as

$$
B_n(s,L)=\frac{(s+q_{n+1})}{2\alpha\kappa_n}A_{n+1}(s)
$$

which can be transformed by using Eq. (17a) to:

$$
B_n(s,x)=\frac{(s+q_{n+1})}{2\alpha\kappa_n}A_{n+1}(s)E^{-s(x-L)/\kappa_n}
$$

and finally, substituting Eq. (18a) in the above one, we obtain

$$
B_n(s,x)=\frac{2^n r_0}{\kappa_n}\left(\prod_{k=1}^{n-1}\left(\frac{\alpha r_k}{s+(r_k+d_k)}+(1-\alpha)\right)\right)E^{-s\left(\sum_{k=0}^{n-1}\tau_k+\frac{x}{\kappa_n}\right)}A_0(s).
$$

Appendix B. algebraic derivation of equation in Section 4.2

The first step in deriving Eq. (19) is to substitute the specific condition for the modified Nordon model on Eqs. (18) obtaining

$$
A_n(s)=\begin{cases} a_0(0)/(s+q) & \text{if } n=0,\\ \dfrac{(2r)^n}{(s+q)^{n+1}}E^{-s((n-1)\tau+\tau_0)}a_0(0) & \text{if } n>0.\end{cases}
$$

Using the following known properties of Laplace transformation:

$$
f(t-t_p)\overset{L}{\leftrightarrow}F(s)E^{-st_p}, \tag{B1}
$$

$$
E^{-at}\frac{t^n}{n!}\overset{L}{\leftrightarrow}\frac{1}{(s+a)^{n+1}}. \tag{B2}
$$

we obtain the Laplace transform

$$
a_n(t)=\begin{cases} a_0(0)E^{-qt} & \text{if } n=0,\\ \dfrac{a_0(0)(2r)^n}{n!}\vartheta[t-(n-1)\tau-\tau_0]^n E^{-q(t-(n-1)\tau-\tau_0)} & \text{if } n>0,\end{cases}
$$

$$
b_n(t,x)=\frac{r}{\kappa_n}\frac{a_0(0)(2r)^n}{n!}\vartheta\left[t-\sum_{k=0}^{n-1}\tau_k-\frac{x}{\kappa_n}\right]^n E^{-q\left(t-\sum_{k=0}^{n-1}\tau_k+\frac{x}{\kappa_n}\right)}.
$$

Note that the step function θ is introduced to prevent t to become negative, since in that region the applied Transformation is not valid and the functions are defined as strictly 0. This also makes biological sense.

Finally, the expression for $b_n^t(t)$ reported in Eq. (19) is obtained by integrating $b_n(t,x)$ in x from 0 to L, using the following table integral:

$$\int E^{-a(t-t_p-x)}(t-t_p-x)^n \mathrm{d}x = \frac{\Gamma(n+1,\ a(t-t_p-x))}{a^{n+1}}.$$

Appendix C. algebraic derivation of equation in Section 4.3

The first step in deriving Eq. (20) is to substitute the specific condition for the extended model on Eq. (18) obtaining

$$A_n(s) = \begin{cases} a_0(0)/(s+q_0) & \text{if } n=0, \\ \dfrac{2^n r_0 r^{n-1}}{(s+q_0)(s+q)^n} E^{-s((n-1)\tau+\tau_0)} a_0(0) & \text{if } n>0, \end{cases}$$

$$B_n(s,x) = \frac{r_0}{\kappa_n}\frac{(2r)^n}{(s+q_0)(s+q)^n} E^{-s\left(\sum_{k=0}^{n-1}\tau_k+\frac{x}{\kappa_n}\right)} a_0(0).$$

We take the inverse Laplace transform using the following known property of Laplace transformation:

$$\int_0^t f(t-x)g(x)\ \mathrm{d}x \overset{L}{\leftrightarrow} F(s)G(s).$$

Combining the latter property with the properties described on Appendix B (Eqs. (B1) and (B2)) we can write for $a_n(t)$:

$$a_n(t) = \begin{cases} a_0(0)E^{-q_0 t} & \text{if } n=0, \\ 2^n r_0 r^{n-1} a_0(0) E^{-q_0(t-(n-1)\tau-\tau_0)} \int_0^{t-(n-1)\tau_k-\tau_0} E^{-(q-q_0)x}\dfrac{x^{n-1}}{(n-1)!}\mathrm{d}x & \text{if } n>0, \end{cases}$$

which can be transformed, by using integral (B3), into

$$a_n(t) = \begin{cases} a_0(0)E^{-q_0 t} & \text{if } n=0, \\ 2^n r_0 r^{n-1} a_0(0)\dfrac{(\Gamma(n)-\Gamma(n,(q-q_0)\theta(t-(n-1)\tau-\tau_0))}{\Gamma(n)(q-q_0)^n} E^{-q_0(t-(n-1)\tau-\tau_0)} & \text{if } n>0. \end{cases}$$

Note that the step function θ is introduced to prevent t to become negative, since in that region the applied transformation is not valid and the functions are defined as strictly 0.

Following a similar procedure $b_n(t,x)$ is obtained as

$$b_n(t,x) = 2^n\frac{r_0}{\kappa_n} r^n\ a_0(0)\frac{\left(\Gamma(n)-\Gamma\left(n,(q-q_0)\theta\left(t-\sum_{k=0}^{n-1}\tau_k-\dfrac{x}{\kappa_n}\right)\right)\right)}{\Gamma(n)(q-q_0)^n} E^{-q\left(t-\sum_{k=0}^{n-1}\tau_k+\frac{x}{\kappa_n}\right)}.$$

Finally to obtain $b_n^L(t)$one integrates $b_n(t,x)$ on x from 0 to L. But to easily get the expression on the form expressed on Eq. (20) one first rewrites Eq. (14a) as

$$b_{n-1}(t,L) = \frac{1}{2\alpha\kappa_{n-1}}\left(\frac{\mathrm{d}a_n(t)}{\mathrm{d}t} + (r_n+d_n)a_n(t)\right).$$

Then one obtains $b_n(t,x)$ by transforming the x coordinate with the time coordinate. Note that, since there is no cell death on the activated compartment, the cells in the position x at time t will be at the position L at time $t+(L-x)/\kappa_n$. Thus $b_n(t,x)$ can be obtained as:

$$b_n(t,x) = \frac{1}{2\alpha\kappa_n}\left(\frac{\mathrm{d}a_{n+1}(t+(L-x)/\kappa_n}{\mathrm{d}t} + q_{n+1}a_{n+1}(t+(L-x)/\kappa_n)\right).$$

Then, integrating on x it is obtained:

$$
\begin{aligned}
b_n^t(t) &= \frac{1}{2\kappa_0}\int_0^L \left(\frac{\mathrm{d}a_{n+1}(t+(L-x)/\kappa_n)}{\mathrm{d}t} + qa_{n+1}(t+(L-x)/\kappa)\right)\mathrm{d}x.\\
&= \frac{1}{2}\int_t^{t+L/\kappa_n}\left(\frac{\mathrm{d}a_{n+1}(x1)}{\mathrm{d}t} + qa_{n+1}(x1)\right)\mathrm{d}x1\\
&= \frac{1}{2}(a_{n+1}(t+L/\kappa_n) - a_{n+1}(t))\\
&\quad + \frac{q}{2}2^{n+1}r_0r^n a_0(0)\int_t^{t+L/\kappa_n}\frac{(\Gamma(n+1)-\Gamma(n+1,(q-q_0)\theta(x1-n\tau-\tau_0)))}{\Gamma(n+1)(q-q_0)^{n+1}}E^{-q_0(x1-n\tau-t_0)}\,\mathrm{d}x1\\
&= \frac{(a_{n+1}(t+\tau_n)-a_{n+1}(t))}{2}\\
&\quad + \frac{2^{n+1}r_0r^n a_0(0)q}{2\Gamma(n+1)(q-q_0)^{n+1}}\int_t^{t+L/\kappa_n}(\Gamma(n+1)-\Gamma(n+1,(q-q_0)\theta(x1-n\,\tau-\tau_0)))E^{-q_0(x1-n\tau-t_0)}\,\mathrm{d}x1
\end{aligned}
$$

which can be finally reduced to Eq. (20) by using the following integral:

$$
\begin{aligned}
\int(\Gamma(n)-\Gamma(n,(q-q_0)(x-c)))E^{-q_0(x-c)}\,\mathrm{d}x = &-\frac{(q-q_0)^n\Gamma(n,q(x-c))}{q^nq_0}\\
&-\left(\frac{(\Gamma(n)-\Gamma(n,(q-q_0)(x-c)))}{q_0}E^{-q_0(x-c)}\right).
\end{aligned}
$$

This is

$$
\begin{aligned}
b_n^t(t) &= \frac{(a_{n+1}(t+\tau_n)-a_{n+1}(t))}{2}\\
&\quad -\frac{(2r)^n r_0a_0(0)}{\Gamma(n+1)}\frac{(\Gamma(n+1,q(t+\tau_n-n\tau-\tau_0)-\Gamma(n+1,q(t-n\tau-\tau_0))}{q^nq_0} - \frac{q}{2}\frac{(a_{n+1}(t+\tau_n)-a_{n+1}(t))}{q_0}\\
&= \frac{(q_0-q)}{2}\frac{(a_{n+1}(t+\tau_n)-a_{n+1}(t))}{q_0} - \frac{(2r)^n r_0a_0(0)}{\Gamma(n+1)}\frac{(\Gamma(n+1,q(t+\tau_n-n\tau-\tau_0)-\Gamma(n+1,q(t-n\tau-\tau_0))}{q^nq_0}.
\end{aligned}
$$

References

Arino, O., 1995. A survey of structured cell population dynamics. Acta Biotheor. 43, 3–25.

Burns, F.J., Tannock, I.F., 1970. On the existence of a Go-phase in the cell cycle. Cell Tissue Kinet. 3 (4), 321–334.

Cantrell, D.A., Smith, K.A., 1984. The interleukin-2 T-cell system: a new cell growth model. Science 224, 1312–1316.

Darzynkiewicz, Z., Crissman, H., Traganos, F., Steinkamp, J., 1982. Cell heterogeneity during the cell cycle. J. Cell. Physiol. 113, 465–474.

Dutton, R.W., Bradley, L.M., Swain, S.L., 1998. T cell memory. Annu. Rev. Immunol. 16, 201–223.

Gett, A.V., Hodgkin, P.D., 2000. A cellular calculus for signal integration by T cells. Nat. Immunol. 1, 239–244.

Givan, A.L., Fisher, J.L., Waugh, M., Ernstoff, M.S., Wallace, P.K., 1999. A flow cytometric methods to estimate the precursor frequencies of cells proliferating in response to specific antigens. J. Immunol. Methods 230, 99–112.

Hasbold, J., Gett, A.V., Rush, J.S., Deenick, E., Avery, D., Jun, J., Hodgkin, P.D., 1999. Quantitative analysis of lymphocyte differentiation and proliferation in vitro using carboxyfluorescein diacetate succinimidyl ester. Immunol. Cell Biol. 77, 516–522.

Iezzi, G., Karjalainen, K., Lanzavecchia, A., 1998. The duration of antigenic stimulation determines the fate of naive and effector T cells. Immunity 8, 89–95.

Jelley-Gibbs, D.M., Lepak, N.M., Yen, M., Swain, S.L., 2000. Two distinct stages in the transition from naive CD4 T cells to effectors, early antigen-dependent and late cytokine-driven expansion and differentiation. J. Immunol. 165, 5017–5026.

Koch, A.L., 1980. Does the variability of the cell cycle result from one or many chance events? Nature 286, 80–82.

Koch, A.L., Schaechte, J., 1962. J. Gen. Microbiol. 29, 435.

Kubitschek, H.E., 1970. The distribution of cell generation times. Cell Tissue Kinet. 4, 113–122.

Lee, W.T., Pasos, G., Cecchini, L., Mittler, J.N., 2002. Continued antigen stimulation is not required during CD4(+) T cell clonal expansion. J. Immunol 168, 1682–1689.

Lodish, H., Baltimore, D., Berk, A., Zipursky, S.L., Matsudaira, P., Darnell, J., 1995. Molecular Cell Biology. Scientific American Books, New York.

Lyons, A.B., Parish, C.R., 1994. Determination of lymphocyte division by flow cytometry. J Immunol. Methods 171, 131–137.

Murali-Krishna, K., Altman, J.D., Suresh, M., Sourdive, D., Zajac, A., Ahmed, R., 1998. In vivo dynamics of anti-viral CD8 T cell responses to different epitopes. An evaluation of bystander activation in primary and secondary responses to viral infection. Adv. Exp. Med. Biol. 452, 123–142.

Nordon, R.E., Nakamura, M., Ramirez, C., Odell, R., 1999. Analysis of growth kinetics by division tracking. Immunol. Cell Biol. 77, 523–529.

Press, W.H., Teukolsky, S.A., Vetterling, W.T., Flannery, B.P., 1999. Numerical recipies in C. Cambridge University Press, Cambridge.

Smith, J.A., Martin, L., 1974. Do cell cycle? Proc. Nat. Acad. Sci. 70, 1263–1267.
Spiegel, M., Liu, J., 1999. Mathematical Handbook of Formulas and Tables. McGraw-Hill, Washington, DC.
Swain, S.L., Croft, M., Dubey, C., Haynes, L., Rogers, P., Zhang, X., Bradley, L.M., 1996. From naive to memory T cells. Immunol. Rev. 150, 143–167.
Usherwood, E.J., Crowther, G., Woodland, D.L., 1999. Apoptotic cells are generated at every division of in vitro cultured T cell lines. Cell Immunol. 196, 131–137.
van Stipdonk, M.J., Lemmens, E.E., Schoenberger, S.P., 2001. Naive CTLs require a single brief period of antigenic stimulation for clonal expansion and differentiation. Nat. Immunol. 2, 423–429.
Veiga-Fernandes, H., Walter, U., Bourgeois, C., McLean, A., Rocha, B., 2000. Response of naive and memory CD8+ T cells to antigen stimulation in vivo. Nat. Immunol. 1, 47–53.